Multiresolution Biomedical Image Registration Using Generalized Information Measures

Mark P. Wachowiak[1], Renata Smolíková[1], and Terry M. Peters[1,2]

[1] Robarts Research Institute
[2] University of Western Ontario
London, ON N6A 5K8 Canada
{mwach, smolikov, tpeters}@imaging.robarts.ca

Abstract. In addition to the widely-used Shannon mutual information, generalized information-theoretic similarity metrics have properties that make them conducive to biomedical image registration. The mutual information based on Havrda-Charvat and Rényi entropy measures are compared to Shannon mutual information, normalized mutual information, the correlation ratio, and other generalized metrics. Single slice/3D registration results on brain and heart volumes show that generalized metrics that deviate slightly from the Shannon metrics can improve registration outcomes based on success rate, and have competitive computation times. The results also suggest that these metrics may be used with Shannon (and other) measures in a complementary manner.

1 Introduction

Many similarity criteria exist for multimodal medical image registration, including statistical measures (e.g. correlation ratio) [1], those based on image features (pattern intensity, gradient difference, gradient cross correlation) [2], and information-theoretic measures (e.g. joint entropy, mutual information) [3, 4], which have been shown to be particularly robust [5]. This paper focuses on generalized information measures, and demonstrates their efficacy within a multiresolution registration framework. They are parameterized by a real number, and typically specialize to Shannon metrics in a limit of their parameter. Some such metrics have already been used for registration [6,7]. The current work applies additional measures to single slice/3D registration for MRI and CT brain and cardiac images, and shows that improvements can be obtained when the generalized and Shannon measures differ only slightly. Such registration is used in motion correction [8], medical research [5], and in aligning 2D projection images to 3D tomographic volumes [2,5]. The current study is limited to rigid registration. Although most tissues are deformable, rigid registration is useful in global alignment prior to local, non-linear registration [9]. It is also employed for locally-constrained registration of images of deformable tissues [8].

After a brief description of generalized metrics, results are presented for experiments on simulated and real medical images. Metrics based on the Rényi

R.E. Ellis and T.M. Peters (Eds.): MICCAI 2003, LNCS 2879, pp. 846–853, 2003.

and Havrda-Charvat entropy definitions are compared with Shannon mutual information (MI), normalized mutual information (NMI), the entropy correlation coefficient (ECC), and the correlation ratio (CR), as well as with other generalized metrics that have appeared in the literature [6,7].

2 Information-Theoretic Similarity Metrics

In the following discussion, let X and Y respectively denote the intensities of the source image and of the corresponding transformed coordinates in the target (reference) volume. Let $p(x_i)$, $i = 1, \ldots, n$, and $p(y_j)$, $j = 1, \ldots, m$ denote the probability distribution of the intensities of X and Y, respectively, and $p(x_i, y_j)$ represent their joint distribution. The Shannon entropy, H, is additive: if X and Y are independent, then $H(X,Y) = H(X) + H(Y)$. Thus, the Shannon mutual information of X and Y is: $I(X,Y) = H(X) + H(Y) - H(X,Y)$. A normalized variant, less sensitive to the size of the source/target overlap, is [10]: $\tilde{I}(X,Y) = \frac{H(X)+H(Y)}{2H(X,Y)}$. Another metric based on Shannon entropy is the entropy correlation coefficient, given as [11]: $\tilde{I}_{ECC}(X,Y) = \sqrt{\frac{2I(X,Y)}{H(X)+H(Y)}}$.

Many generalized entropy definitions exist. Most have the property that they approach the Shannon entropy in some limit of their parameter(s). One of the earliest such definitions is that of Rényi [12]: $R_\alpha(X) = \frac{1}{1-\alpha} \ln \sum_{i=1}^{n} p^\alpha(x_i)$, $\alpha \in \mathcal{R} - 1$. The Rényi entropy becomes the Shannon entropy as $\alpha \to 1$. Like H, R_α is additive, and therefore a measure of Rényi information, I_α^R, is [7]:

$$I_\alpha^R(X,Y) = R_\alpha(X) + R_\alpha(Y) - R_\alpha(X,Y). \tag{1}$$

A non-logarithmic form of entropy is proposed by Havrda-Charvat [13]: $S_\alpha(X) = \frac{1}{1-\alpha}\left(\sum_{i=1}^{n} p^\alpha(x_i) - 1\right)$, $\alpha \in \mathcal{R} - 1$. This entropy becomes Shannon entropy as $\alpha \to 1$. S_α, functionally similar to the Tsallis entropy [14], is non-additive. However, if X and Y are independent, then $S_\alpha(X,Y) = S_\alpha(X) + S_\alpha(Y) + (1-\alpha)S_\alpha(X)S_\alpha(Y)$. Thus, an information measure information using S_α, I_α^S (which becomes I for $\alpha = 1$), is [14]:

$$I_\alpha^S(X,Y) = S_\alpha(X) + S_\alpha(Y) + (1-\alpha)S_\alpha(X)S_\alpha(Y) - S_\alpha(X,Y). \tag{2}$$

Some generalized measures have been applied to biomedical image registration, including I_α and M_α information [6]:

$$I_\alpha(X,Y) = \frac{1}{\alpha(\alpha-1)}\left(\sum_{i=1}^{n}\sum_{j=1}^{m} \frac{p^\alpha(x_i,y_j)}{(p(x_i)p(y_j))^{\alpha-1}} - 1\right), \tag{3}$$

and

$$M_\alpha(X,Y) = \sum_{i=1}^{n}\sum_{j=1}^{m} |p^\alpha(x_i,y_j) - (p(x_i)p(y_j))^\alpha|^{1/\alpha}. \tag{4}$$

These various information measures exhibit different behaviours as X and Y come into alignment (become more dependent). This behaviour is illustrated in Fig. 1 for I, $\tilde{I}_{ECC}$, and for various parameters of I_α^S and M_α. In the figure, the metrics were computed from 8-bit joint distributions ranging from complete dependence ($p(x_i, y_j) = 1/256$ for $i = j$, and 0 otherwise) to complete independence ($p(x_i, y_j) = 1/256^2$ for $i, j = 1, 2, \ldots, 256$). Metric curve behaviour is related to its parameter value. For instance, the M_α metric for $\alpha = 0.25$ is more sensitive to changes in independence as the images approach correct alignment, whereas is it not sensitive for large misalignments. The converse is true for $\alpha = 2$. The shape of the curves approach that of I as the parameter values approach 1. The functional behaviour of these metrics can be exploited to improve registration outcomes. Henceforth, it is assumed that the similarity metric function attains its maximum at correct alignment, although exceptions do exist [5].

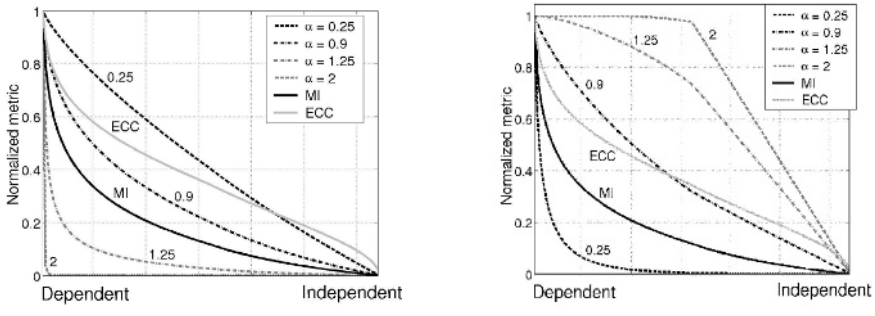

Fig. 1. Curves of MI, ECC, and generalized metrics representing change from dependence (alignment) to independence. (a) I_α^S information. (b) M_α information.

3 Methods

3.1 Images

All experiments were rigid body multimodal registrations of 2D slices to 3D volumes. The data consisted of: 1: Simulated PD MRI images of a brain with multiple sclerosis lesions registered to a corresponding T1 MRI volume of a normal brain with 5% noise, and 2: with 9% noise (BrainWeb, Montreal Neurological Institute) [15] (Fig. 2). 3: 2D MRI to 3D CT registration of brain images obtained through the NLM-NIH Visible Human Project (VHP) female dataset (Fig. 3, (a) and (b)). 4: 2D MRI to 3D CT registration of whole-heart images obtained from VHP male dataset (Fig. 3, (c) and (d)). Beam-hardening artifacts were present in this CT volume, which also had low contrast even after enhancement. As the voxel size was known, the volumes and corresponding slices were resampled to be isotropic and equal in resolution to eliminate scaling transformation parameters [8]. The data are described in detail in Table 1.

Table 1. Data used in registration experiments.

Volume	Description	Voxel size (mm)	Volume size	Image modality	Image size (# images)	Original pixel size (mm)	Source
1	T1 MRI Normal Brain 5% noise	1.0	$217 \times 181 \times 181$	PD MRI MS lesions 0% noise	101×101 (4)	1.0	BrainWeb
2	T1 MRI Normal Brain 9% noise	1.0	$217 \times 181 \times 181$	PD MRI MS lesions 0% noise	101×101 (4)	1.0	BrainWeb
3	CT Head Female	0.448	$440 \times 440 \times 246$	PD MRI	161×161 (1) 201×201 (3) 281×281 (1)	0.859	VHP
4	CT Heart Male	0.9375	$301 \times 301 \times 305$	PD MRI	201×201 (4)	1.875	VHP

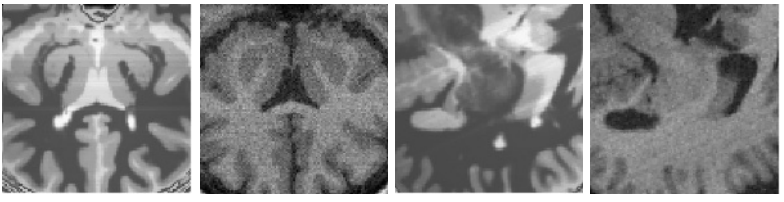

(a) (b) (c) (d)

Fig. 2. (a) and (c) Simulated PD MRI MS lesion brain images. (b) and (d) Corresponding slice in T1 volume (9% noise).

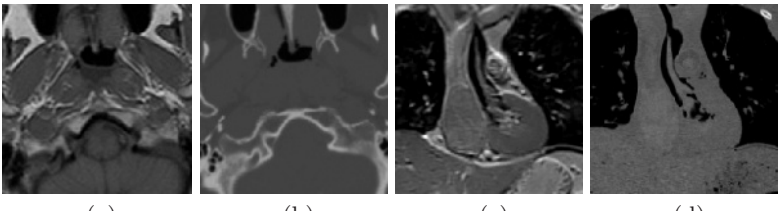

(a) (b) (c) (d)

Fig. 3. (a) PD MRI head image. (b) Corresponding slice from CT volume. (c) PD MRI heart image. (d) Corresponding slice from CT volume.

3.2 Registration Controls and Performance Metrics

To test the proposed similarity metrics, translations along the x-, y-, and z- axes and rotations about the x-, y-, and z-axes were determined. For all experiments, ground truth transformations were known. The initial orientations were chosen using a protocol similar to [2]. There were six initial positions from ground truth:

$\pm 4°$ rotation error for translation errors of 5 and 10 mm (denoted as positions 1 and 2), $\pm 8°$ and 15 mm (position 3), $\pm 12°$ and 20 mm (position 4), $\pm 16°$ and 25 mm (position 5), and $\pm 20°$ and 30 mm translation error (position 6). The rotation errors were applied on all three axes. The image centres were placed at four locations for each distance. Thus, $8 \times 4 \times 6 = 192$ registrations were performed for each slice and for each metric.

Probability density estimation is critical for accurate metric computation and registration accuracy. Parzen windows [4] and histograms [3] have been used in previous studies. The latter approach was adopted in the current work. For the data sets in this study, using 64 bins generally produced a smooth representation of the density, while retaining important intensity features [3,5]. During resampling, partial volume interpolation [3] was employed. Optimization was performed with Powell's method, a direct local optimization technique used in many registration studies [3,6,16]. I, $\tilde{I}$, $\tilde{I}_{ECC}$, CR, I^R_α, I^S_α, and I_α for $\alpha \in \{0.25, 0.5, 0.9, 1.1, 1.25, 1.5, 2\}$, and M_α for $\alpha \in \{0.2, 0.5, 0.9, 1.1, 1.25\}$ were compared. Parameters lower than 0.25 and higher than 2 exhibit numerical inaccuracies and rough registration functions. Values for the latter two metrics were similar to those in [6]. For multiresolution registration, the images were subsampled in all dimensions. (Blurring prior to subsampling does not necessarily improve performance, and increases computation time [16].) The result from one resolution was used as the initial orientation in the next higher resolution. The VHP head images were successively registered at 4- and 2-voxel subsampling, and then at full resolution. The lower-resolution BrainWeb and VHP heart images were first registered with 2-voxel subsampling, followed by full resolution.

The metrics were judged with respect to: 1: The success rate (ratio of correct registrations). A registration is considered correct if the Euclidean distance between the final and ground truth translation parameters is less than 2.5 mm, and if the angle between the planes formed by the ground truth and final transformations is less than 2°, and 2: the efficiency, or average number of function (similarity metric) evaluations for successful registrations.

4 Results

The success rates and mean translation error (MTE), in mm, are displayed in Tables 2 and 3. As this rate was less than 0.50 for positions 5 and 6 for all metrics, only positions 1–4 are shown, along with the overall rate for positions 1–3 (5–15 mm). For the generalized measures, the two best parameters are displayed. The mean number of function evaluations is shown in Table 4, as is the mean time for correct registrations (running serially on Intel ®Itanium ®900 MHz processors) for image sizes of 101×101 voxels (Volume 2) and 201×201 voxels (Volume 4).

I^S_α and I^R_α had the highest success rate for the BrainWeb and VHP heart volumes. For the the VHP head volume, I and $\tilde{I}_{ECC}$ also had high success rates. CR generally had fewer satisfactory registrations than the information-theoretic measures. The heart volume had the lowest success rate and highest MTE, possibly due to low image resolution, beam-hardening artifacts, and low

CT contrast. The CR and M_α metrics had the highest MTE, but the mean translation errors among the remaining metrics were similar. For the generalized metrics, the best results occurred for α between 0.9 and 1.5. I^S_α generally had higher success rates than I_α and M_α. Among the Shannon metrics, $\tilde{I}$ had the lowest success rate for all volumes, although it was the most efficient, along with $\tilde{I}_{ECC}$ (Table 4). I and the generalized metrics required the most function evaluations, with no noticeable difference in their efficiencies. Registrations using NMI and CR were the fastest (Table 4), and were the slowest with I and M_α. Registration using I^S_α and I^R_α was generally slightly faster than with MI.

Table 2. Success rate for positions 1–4 and overall success rate and mean translation error (MTE) in mm for Volumes 1 and 2. Overall success rate values higher than that for Shannon MI are shown in boldface.

	Volume 1						Volume 2					
Metric	1	2	3	4	Overall	MTE	1	2	3	4	Overall	MTE
I	0.98	0.71	0.17	0.07	0.62	0.25 ± 0.43	0.95	0.67	0.13	0.02	0.58	0.32 ± 0.44
$\tilde{I}$	0.95	0.64	0.13	0.03	0.57	0.27 ± 0.42	0.91	0.64	0.13	0.01	0.56	0.40 ± 0.47
$\tilde{I}_{ECC}$	0.99	0.72	0.18	0.03	0.63	0.26 ± 0.43	0.94	0.73	0.20	0.02	0.62	0.33 ± 0.43
CR	0.91	0.66	0.16	0.03	0.57	0.51 ± 0.46	0.84	0.67	0.14	0.04	0.55	0.58 ± 0.47
$I^S_{1.5}$	1.00	0.84	0.31	0.11	**0.72**	0.28 ± 0.43	0.99	0.66	0.30	0.09	**0.65**	0.27 ± 0.43
I^S_2	0.99	0.80	0.42	0.09	**0.74**	0.33 ± 0.45	0.99	0.71	0.26	0.09	**0.65**	0.33 ± 0.42
$I^R_{1.25}$	1.00	0.70	0.26	0.06	**0.65**	0.26 ± 0.42	0.97	0.71	0.23	0.06	**0.64**	0.29 ± 0.44
$I^R_{1.5}$	1.00	0.73	0.25	0.05	**0.66**	0.34 ± 0.42	0.98	0.62	0.20	0.06	0.60	0.31 ± 0.43
$I_{0.9}$	0.98	0.71	0.19	0.01	0.63	0.24 ± 0.41	0.95	0.70	0.18	0.01	0.61	0.33 ± 0.44
$I_{1.1}$	0.98	0.73	0.20	0.04	**0.64**	0.25 ± 0.42	0.95	0.68	0.18	0.02	0.60	0.31 ± 0.49
$M_{0.5}$	0.93	0.66	0.09	0.02	0.58	0.37 ± 0.44	0.93	0.66	0.09	0.02	0.56	0.64 ± 0.45
$M_{0.9}$	0.98	0.67	0.16	0.02	0.60	0.38 ± 0.44	0.95	0.63	0.14	0.02	0.57	0.55 ± 0.40

Table 3. Success rate for positions 1–4 and overall success rate and mean translation error (MTE) in mm for Volumes 3 and 4. Overall success rate values higher than that for Shannon MI are shown in boldface.

	Volume 3						Volume 4					
Metric	1	2	3	4	Overall	MTE	1	2	3	4	Overall	MTE
I	1.00	0.98	0.58	0.17	0.85	0.30 ± 0.20	0.77	0.80	0.63	0.51	0.73	1.33 ± 0.37
$\tilde{I}$	0.98	0.92	0.43	0.09	0.78	0.29 ± 0.16	0.63	0.61	0.39	0.31	0.55	1.43 ± 0.38
$\tilde{I}_{ECC}$	1.00	0.94	0.62	0.18	0.85	0.27 ± 0.16	0.70	0.67	0.59	0.41	0.65	1.33 ± 0.36
CR	0.91	0.76	0.30	0.08	0.66	0.63 ± 0.25	0.63	0.60	0.48	0.28	0.57	1.37 ± 0.32
$I^S_{1.1}$	1.00	0.97	0.66	0.19	**0.88**	0.29 ± 0.20	0.80	0.83	0.63	0.45	**0.75**	1.21 ± 0.30
$I^S_{1.25}$	1.00	0.97	0.59	0.20	0.85	0.28 ± 0.20	0.81	0.75	0.57	0.43	0.71	1.19 ± 0.32
$I^R_{1.1}$	1.00	0.95	0.63	0.18	**0.86**	0.29 ± 0.17	0.84	0.82	0.61	0.48	**0.76**	1.21 ± 0.31
$I^R_{1.25}$	1.00	0.95	0.55	0.17	0.83	0.35 ± 0.24	0.81	0.84	0.63	0.46	**0.76**	1.15 ± 0.35
$I_{1.25}$	1.00	0.98	0.55	0.15	0.84	0.28 ± 0.21	0.78	0.74	0.55	0.47	0.69	1.23 ± 0.36
$I_{1.5}$	1.00	0.93	0.56	0.16	0.83	0.27 ± 0.20	0.76	0.66	0.50	0.39	0.69	1.22 ± 0.40
$M_{0.5}$	0.95	0.90	0.41	0.14	0.77	0.52 ± 0.23	0.64	0.64	0.51	0.37	0.60	1.35 ± 0.34
$M_{0.9}$	0.98	0.84	0.45	0.10	0.76	0.53 ± 0.26	0.63	0.61	0.45	0.30	0.56	1.27 ± 0.37

Table 4. Mean number of function evaluations for satisfactory registrations (×1000).

Metric	Vol. 1	Vol. 2	Vol. 3	Vol. 4	Time (sec) (101 × 101 voxels)	Time (sec) (201 × 201 voxels)
I	1.38 ± 0.30	1.37 ± 0.31	1.76 ± 0.41	1.16 ± 0.22	26.39 ± 8.69	71.60 ± 19.62
$\tilde{I}$	0.91 ± 0.19	0.86 ± 0.19	1.05 ± 0.19	0.66 ± 0.15	16.17 ± 4.26	38.04 ± 12.30
$\tilde{I}_{ECC}$	1.25 ± 0.29	1.27 ± 0.29	1.52 ± 0.35	1.05 ± 0.25	24.17 ± 7.67	65.07 ± 19.93
CR	1.28 ± 0.31	1.29 ± 0.32	1.85 ± 0.36	1.14 ± 0.29	17.45 ± 6.03	63.50 ± 20.89
$I^S_{1.1}$	1.37 ± 0.35	1.39 ± 0.32	1.72 ± 0.37	1.15 ± 0.30	19.41 ± 6.95	67.65 ± 23.13
$I^S_{1.25}$	1.34 ± 0.32	1.36 ± 0.33	1.70 ± 0.35	1.16 ± 0.29	19.51 ± 7.40	65.47 ± 25.29
$I^S_{1.5}$	1.36 ± 0.35	1.40 ± 0.34	1.68 ± 0.34	1.68 ± 0.28	20.52 ± 8.39	67.96 ± 24.67
I^S_2	1.39 ± 0.32	1.40 ± 0.32	1.75 ± 0.35	1.23 ± 0.28	20.65 ± 6.99	70.14 ± 24.91
$I^R_{1.1}$	1.34 ± 0.32	1.34 ± 0.30	1.66 ± 0.35	1.17 ± 0.32	18.43 ± 6.71	65.14 ± 22.38
$I^R_{1.25}$	1.34 ± 0.34	1.39 ± 0.33	1.63 ± 0.30	1.12 ± 0.28	20.02 ± 7.83	64.33 ± 25.91
$I^R_{1.5}$	1.34 ± 0.33	1.37 ± 0.34	1.65 ± 0.35	1.13 ± 0.27	19.81 ± 7.86	66.01 ± 25.15
I^R_2	1.28 ± 0.29	1.30 ± 0.26	1.63 ± 0.27	1.04 ± 0.26	18.29 ± 5.32	59.84 ± 19.91
$I_{0.9}$	1.40 ± 0.35	1.42 ± 0.33	1.69 ± 0.35	1.22 ± 0.30	19.82 ± 7.11	65.93 ± 23.12
$I_{1.1}$	1.39 ± 0.33	1.39 ± 0.32	1.71 ± 0.30	1.16 ± 0.26	19.12 ± 6.84	65.73 ± 21.31
$I_{1.25}$	1.38 ± 0.34	1.42 ± 0.31	1.75 ± 0.37	1.21 ± 0.27	20.43 ± 7.21	67.56 ± 19.11
$I_{1.5}$	1.43 ± 0.30	1.42 ± 0.30	1.81 ± 0.38	1.22 ± 0.29	20.60 ± 6.47	70.54 ± 20.36
$M_{0.5}$	1.74 ± 0.39	1.67 ± 0.33	2.07 ± 0.36	1.33 ± 0.30	25.93 ± 7.11	84.24 ± 24.18
$M_{0.9}$	1.47 ± 0.30	1.47 ± 0.29	1.77 ± 0.31	1.19 ± 0.31	22.68 ± 6.42	64.86 ± 18.04
$M_{1.1}$	1.39 ± 0.29	1.40 ± 0.26	1.72 ± 0.31	1.13 ± 0.29	21.87 ± 6.14	66.70 ± 22.38

5 Discussion and Conclusions

For the generalized metrics, parameter values close to 1 (at which they resemble Shannon metrics) had the highest success rate. Parameters much different than unity have rough similarity metric functions, and are difficult to optimize [6,7]. The I^R_α and I^S_α metrics, with α slightly greater than 1 ($\alpha \in [1.1, 2]$), were the overall best performers, with about the same efficiency as I. Misregistrations often result from entrapment in local extrema of the registration function, to which local optimization methods are susceptible. Many of the generalized metrics have smoother registration surfaces than MI [7], and are more sensitive to changes in dependence (Fig. 1). MI and ECC generally had higher success rates than NMI.

Although generalized metrics have been shown to be robust similarity criteria for biomedical image registration, parameter choice greatly affects performance. Utilizing different measures at different resolutions (a similar suggestion was made in [6]), may further improve performance. The Shannon metrics are generally accurate and efficient for registrations with initial orientations already close to alignment. Therefore, these metrics could be used in the later registration stages, after optimization of generalized metrics. Registration is also heavily affected by the optimization method. Although Powell's method is generally robust and widely used in registration applications, it is also susceptible to entrapment in local minima, which may have caused the low accuracy of the metrics for $\alpha < 1$. Performance could also potentially be enhanced with global optimization (for distant initial orientations) combined with gradient-based local optimization or robust direct methods, and by adaptive adjustment of metric parameters. Future work also includes testing the metrics on a wide variety of clinical data, extension to registering 3D source data sets, and adaptation to non-linear registration.

Acknowledgements. The authors thank Dr. Maria Drangova (Robarts Research Institute), for valuable suggestions. Data were provided through NLM-NIH Visible Human Project and BrainWeb. M. Wachowiak also thanks his former advisor, Dr. Adel S. Elmaghraby (University of Louisville, Louisville, KY USA). Funding for this project was provided by SHARCNet, NSERC (R3146-A02), CIHR (MT 14735), (MT 11540), and (MGP 49536).

References

1. Roche, A., Malandain, G., Pennec, X., Ayache, N.: The Correlation Ratio as a New Similarity Measure for Multimodal Image Registration. LNCS 1496: MICCAI'98 (1998) 1115–1124.
2. Hipwell, J. H., Penney, G. P., Cox, T. C., Byrne, J. V., Hawkes, D. J.: 2D-3D Intensity Based Registration of DSA and MRA – A Comparison of Similarity Measures. LNCS 2489:MICCAI'02 (2002) 501–508.
3. Maes, F., Collignon, A., Vandermeulen, D., Marchal, G., Suetens, P.: Multimodality Image Registration by Maximization of Mutual Information. IEEE Trans. Med. Imaging 16 (1997) 187–198.
4. Wells III, W. M., Viola, P., Atsumi, H., Nakajima, S., Kikinis, R.: Multi-Modal Volume Registration by Maximization of Mutual Information. Med. Image Anal. 1 (1996) 35–51.
5. Hill, D. L. G., Batchelor, P. G., Holden, M., Hawkes, D. J.: Medical Image Registration. Phys. Med. Biol. 46 (2001) R1–R45.
6. Pluim, J. P. W., Maintz, J. B. A, Viergever, M. A.: f-Information Measures in Medical Image Registration. Proc. SPIE 4322 (2001) 579–587.
7. Wachowiak, M. P., Smolíková, R., Tourassi, G. D., Elmaghraby, A. S.: Similarity Metrics Based on Non-additive Entropies for 2D-3D Multimodal Biomedical Image Registration. Proc. SPIE 5032 (2003) 1090–1100.
8. Hutton, B. F., Braun, M., Thurfjell, L., Lau, D. Y. H.: Image Registration: An Essential Tool for Nuclear Medicine. Eur. J. Nucl. Med. 29(4) (2002) 559–577.
9. McLeish, K., Hill, D. L. G., Atkinson, D., Blackall, J. M., Razavi, R.: A Study of the Motion and Deformation of the Heart Due to Respiration. IEEE Trans. Med. Imaging 21(9) (2002) 1142–1150.
10. Studholme, C., Hill, D. L. G., Hawkes, D. J.: An Overlap Invariant Entropy Measure of 3D Medical Image Alignment. Pattern Recognition 32 (1999) 71–86.
11. Astola, J., Virtanen, I.: Entropy Correlation Coefficient, a Measure of Statistical Dependence for Categorized Data. In Proc. Univ. Vaasa, Finland, Discussion papers 44 (1982) 1–12.
12. Rényi, A.: Probability Theory. North-Holland, Amsterdam (1970).
13. Havrda, J. H., Charvat, F.: Quantification Methods of Classification Processes: Concepts of Structural α Entropy. Kybernetica 3 (1967) 30–35.
14. Vidiella-Barranco, A.: Entanglement and Nonextensive Statistics. Physics Letters A 260 (1999) 335–339.
15. Kwan, R. K. S., Evans, A. C., Pike, G. B.: MRI Simulation-Based Evaluation of Image Processing and Classification Methods. IEEE Trans. Med. Imaging 18 (1999) 1085–1097.
16. Pluim, J. P. W., Maintz, J. B. A., Viergever, M. A.: Mutual Information Matching in Multiresolution Contexts. Image and Vision Computing 19 (2001) 45–52.